American Mineralogist, Volume 91, pages 353–365, 2006

TEM imaging and analysis of microinclusions in diamonds: A close look at diamond-growing fluids

OFRA KLEIN-BENDAVID,[1,*] RICHARD WIRTH,[2] AND ODED NAVON[1]

[1]Institute of Earth Sciences, The Hebrew University of Jerusalem, Jerusalem, 91904, Israel
[2]GeoForschungsZentrum, Potsdam, Telegrafenberg, Div.4, D-14473, Potsdam, Germany

ABSTRACT

Fluid-bearing microinclusions in diamonds (<1 μm) provide a unique source of information on the diamond-forming medium. Transmission electron microscopy (TEM) investigation of such microinclusions enables the detailed study of their size, external habit, internal morphology, and mineralogy, and yields information on the chemical composition and crystallography of the included phases. Here we present a detailed TEM examination of microinclusions in four fibrous diamonds from Canada and Siberia, each with a distinctive inferred original fluid composition. Most microinclusions contain multi-phase assemblages that include carbonate, halide, apatite, possible pyroxene, and high-silica mica (6.8–7.7 Si atoms per formula unit) whose composition lies along the phlogopite–Al-celadonite join. The TEM results, together with the tight range of composition detected by electron probe microanalysis (EPMA) and the volatiles detected by infrared (IR) spectroscopy, suggest that the microinclusions trapped a uniform, dense, supercritical fluid and that the crystallized minerals grew as secondary phases during cooling.

Carbonates appear in all assemblages, together with either halides or silicates, indicative of the importance of carbonatitic high-density fluid during diamond growth and fluid evolution. The presence of halide-carbonate or silicate-carbonate assemblages is in agreement with the bulk composition of the microinclusions as detected by EPMA. The high K content of some microinclusions detected by EPMA cannot be accounted for by the solid phases analyzed by TEM. This discrepancy suggests that K is concentrated in the residual fluid that is lost during TEM sample preparation. In addition to microinclusions, large cavities containing amorphous phases were found in the inner parts of one Siberian and one Canadian diamond. An Al-rich phase is the most abundant, and it is accompanied by Ca-rich and Si-rich phases. These phases may be explained by amorphization of crystalline phases. A breakdown of a single melt into three immiscible components is less likely.

Keywords: Crystal structure, high-density fluid, high-silica mica, carbonate, halide, secondary minerals, multi-phase assemblage

INTRODUCTION

Inclusions in diamonds provide a unique opportunity to investigate the mantle rocks in which diamonds are formed and the fluids from which diamonds crystallize. The strength of diamond and its low reactivity in a silicate environment allow encapsulation of trapped material and preservation of its original composition. Mineral inclusions range in size from tens of nanometers to almost a millimeter, and most indicate a peridotitic or eclogitic paragenesis. Mineral assemblages consist mainly of silicates and chromites with minor oxide, sulfide, and carbonate minerals (Meyer 1987; Harris 1992). Temperatures and pressures calculated from phase equilibria indicate that most diamonds grow at 900–1300 °C and at depth of 150–200 km (Meyer 1987; Harris 1992).

Based on cathodoluminescence (CL) images of the internal structure of diamonds (Milledge et al. 1984; Bulanova 1995), the low density of dislocations (Sunagawa 1984), and the association of diamonds with cracks within their host xenoliths (Taylor et al. 2000), it was concluded that most natural diamonds grow from fluids. The compositions of such fluids can be examined by studying fluid-bearing microinclusions. Such microinclusions are not common, but they can be found in fibrous cubic diamonds, in the fibrous coats of coated diamonds, and as internal clouds in octahedral diamonds (Navon 1999). The microinclusion-bearing zones are populated by millions of sub-micrometer inclusions.

Transmission electron microscopy (TEM) is an ideal tool for the investigation of microinclusions in diamonds. It yields information on their size, external habit, internal morphology, and mineralogy as well as on the chemical composition and crystallography of the included phases. Previous TEM studies revealed the presence of apatite, ankerite, high- and low-Ca carbonate, quartz, biotite, and an unidentified mica (Lang and Walmsley 1983; Guthrie et al. 1991; Walmsley and Lang 1992a, 1992b). In most cases, two or more of the above phases coexist in individual inclusions. The minerals always occupy only a fraction of the inclusion volume, the rest is occupied by a fluid phase. The presence of such fluid was suggested by Guthrie et al. (1991), who observed motion of the secondary crystals within intact microinclusions upon condensing the electron beam. This observation

* E-mail: ofrak@vms.huji.ac.il, oded.navon@vms.huji.ac.il

is also consistent with the presence of water and carbonate in the infrared spectra of microinclusion-rich zones. The uniform compositions of the microinclusions in individual diamonds, as detected by electron-probe microanalysis (EPMA) led to the conclusion that the microinclusions originally were trapped as a supercritical, volatile-rich fluid (Schrauder and Navon 1994). At the pressures and temperatures of the diamond stability field, the silicate melts, carbonatitic melts, and hydrous fluids are beyond a second critical point and are fully miscible (Wyllie and Ryabchikov 2000). The trapped fluid is a highly concentrated, high-density fluid (HDF) and is similar in its composition to subcritical melts. This HDF needs to be distinguished from the residual, low-density fluid that is left in the microinclusions after the secondary mineral phases crystallized from the HDF during cooling. In many cases, the inclusions are penetrated during the milling of the TEM sample and the residual low-density fluid is lost. Occasionally, the inclusion is kept intact, allowing the observation of the low-density fluid as well (Guthrie et al. 1991).

Whereas TEM provides data on individual secondary phases, EPMA yields the bulk compositions of the microinclusions. The bulk compositions can be grouped into three different "end-members" (Schrauder and Navon 1994; Izraeli et al. 2001): (1) a hydrous-silicic end-member rich in water, Si, Al, and K; (2) a carbonatitic end-member rich in carbonate, Mg, Ca, Fe, K, and Na; and (3) a hydrous-saline end-member rich in Cl, K, and Na. Water and carbonates, detected by Fourier transform infrared (FTIR) spectroscopy (Chrenko et al. 1967; Navon et al. 1988), are the main volatile components. All compositions are rich in K and many other incompatible elements (Schrauder et al. 1996).

Microinclusions in diamond represent an exceptional crystallization environment in the mantle, rich in alkalis, chlorine, carbonate, and water under high internal pressure (Navon 1991). Investigation of the phases that crystallized inside the microinclusions provides a rare view into the nature of diamond-forming fluids and into a unique crystallization environment. Here we present a detailed TEM investigation of the mineralogy of the secondary mineral phases in four representative diamonds, each displaying a different compositional range of the original HDF.

Samples and methods

Sample descriptions

Three diamonds from the Diavik mine, Lac de Gras, Slave Craton, Canada, were analyzed. Diamond ON-DVK-272 has an octahedral transparent core surrounded by an opaque, gray, fibrous coat (Fig. 1a). Diamond ON-DVK-281, is a gray fibrous cube (Fig. 1b). Diamond ON-DVK-294 has an octahedral transparent core surrounded by alternating cavity-rich layers and greenish fibrous zones (Fig. 1c, see also Klein-BenDavid et al. 2004). One fibrous cube, UB-5-41, from the Yubileinaya mine in Siberia with a central microinclusion-rich zone, was also analyzed (Fig. 1d).

FTIR and EPMA analysis

Before studying the microinclusions by TEM, polished plates (0.4–1.2 mm thick) of the four diamonds were characterized using optical microscopy, CL (Gatan miniCL), and FTIR (Bruker IRscope II microscope coupled to a Nicolet 740 spectrometer). Individual microinclusions were analyzed using EPMA (JEOL JXA 8600 probe). Analytical conditions and procedures for the EPMA, CL, and IR methods are described in detail by Izraeli et al. (2001, 2004) and Klein-BenDavid et al. (2004). The $CO_2/(CO_2 + H_2O)$ ratio of the material trapped in the diamond is inferred using the height of the water and carbonate bands at 3420 and 1448 cm^{-1} respectively (Fig. 2) and the absorption coefficients of Navon et al. (1988). The precision of the ratio is better than 10%.

EPMA provided the relative abundance of Si, Ti, Al, Fe, Mg, Ca, Ba, Na, K, P, and Cl. The microinclusions detected by EPMA are shallow, subsurface inclusions and are fully surrounded by carbon matrix. They could be seen in back-scattered electron imaging and were analyzed by energy dispersive spectrometry (EDS). The inclusions are smaller than the volume activated by the electron beam. Moreover, as much as 30% of the microinclusion is filled by low electron density elements (in water and carbonate), thus the analyses comprise mostly carbon and only ~4% of the other elements, resulting in low totals. Izraeli et al. (2004) demonstrated that in spite of the low totals, precision is good (about 10% relative), and they estimated accuracy as better then 15% for the major elements. Each EPMA analysis represents a single analyzed microinclusion.

To combine FTIR and EPMA data we assumed that chloride, phosphate, and carbonate ions balance the charge of Ca, Mg, Fe, Ba, Na, and K. Silicon, Al, and Ti are assumed to form silicates and be balanced by O. Thus, $CO_3^{2-} = Ca^{2+} + Mg^{2+} + Fe^{2+} + Ba^{2+} + 0.5Na^{+} + 0.5K^{+} - 0.5Cl^{-} - 1.5PO_4^{3-}$. The water may than be calculated based on the $CO_2/(CO_2 + H_2O)$ ratio determined from the IR spectra.

Sample preparation for TEM analysis

Sample preparation has always been an obstacle for TEM analysis of diamond microinclusions. Thinning the diamond to ~200 nm led to loss of much of the microinclusion filling (Lang and Walmsley 1983). We used a focused ion beam (FIB) of Ga ions, accelerated to 30 kV to mill a small volume of diamond and to extract a thin foil ($10 \times 15 \times 0.2$ µm) of microinclusion-bearing diamond (Figs. 1e and 1f). FIB milling was conducted in the oil-free, high-vacuum chamber of an FEI FIB2000 instrument (GFZ, Potsdam). Before milling, a 2 µm Pt layer was deposited on the diamond from a high-purity $C_6H_{16}Pt$ gas to protect the sample surface. After milling, the foil was cut (Fig. 1f), extracted, and placed on a carbon-coated Cu grid. Details of the FIB milling and TEM foil preparation are given in Wirth (2004) and references therein.

Chemical analysis and electron diffraction. TEM analysis and imaging were conducted using a Philips CM200 microscope with a LaB_6 electron source. The electron acceleration voltage was 200 kV. Electron energy-loss spectroscopy (EELS) was done using a Gatan imaging filter (GIF). Foil thickness was measured using the zero-loss spectrum and the total EEL spectrum (Egerton 1996). The electron inelastic mean free path in diamond was calculated using the formalism given in Egerton (1996). Chemical analysis was carried out using an energy dispersive X-ray spectrometer (EDAX) with an ultrathin window, spot size of 3.8 nm, specimen tilt of 20°, and counting time of 200 s. All analytical data were corrected for fluorescence and absorbtion using the foil thickness as determined using EELS (although, the thickness of the analyzed material in the microinclusion may be smaller due to solid and fluid loss from the exposed microinclusion upon foil preparation).

EDAX spectra were quantified using the ratio technique of Cliff and Lorimer (1975) where $C_a/C_b = K_{ab}(I_a/I_b)$. C_a and C_b are concentrations and I_a and I_b are the intensities of elements a and b, respectively. The K_{ab} factor depends on the matrix and on the fluorescence yield of different elements. The total error strongly depends on the counting statistics and hence the concentration of the various elements. The total error estimate for major components (>10 wt%) is 2–5%, for minor elements (5–10 wt%) is 7–15% and for lower concentrations it may exceed 50%. Total error includes the errors in the K_{ab} factors, the counting statistics and the unknown microinclusion thickness (which may be smaller than the sample thickness). Sodium concentrations could not be measured due to interference of its $K\alpha$ peak with the Ga$L\alpha$ peak.

Results

Results from FTIR and EPMA

Infrared spectra were obtained from only three diamonds, as diamond ON-DVK-294 is opaque. All three are IaA diamonds (carrying pairs of N atoms) as is common for microinclusion bearing diamonds (Fig. 2). Additional bands due to absorption by the material trapped in the inclusions include water bands at 3420 and 1640 cm^{-1} and carbonate bands at 1448 and 880 cm^{-1}. The IR spectrum of diamond ON-DVK-281 reveals additional bands at 460, 832, 1000, 1020, 1072, and 1095 cm^{-1} (Fig. 3a). They resemble the absorption bands of mica. The H_2O to carbonate ratio was calculated from the relative intensities of the bands at 3420 cm^{-1} and 1448 cm^{-1}, using the absorption coef-

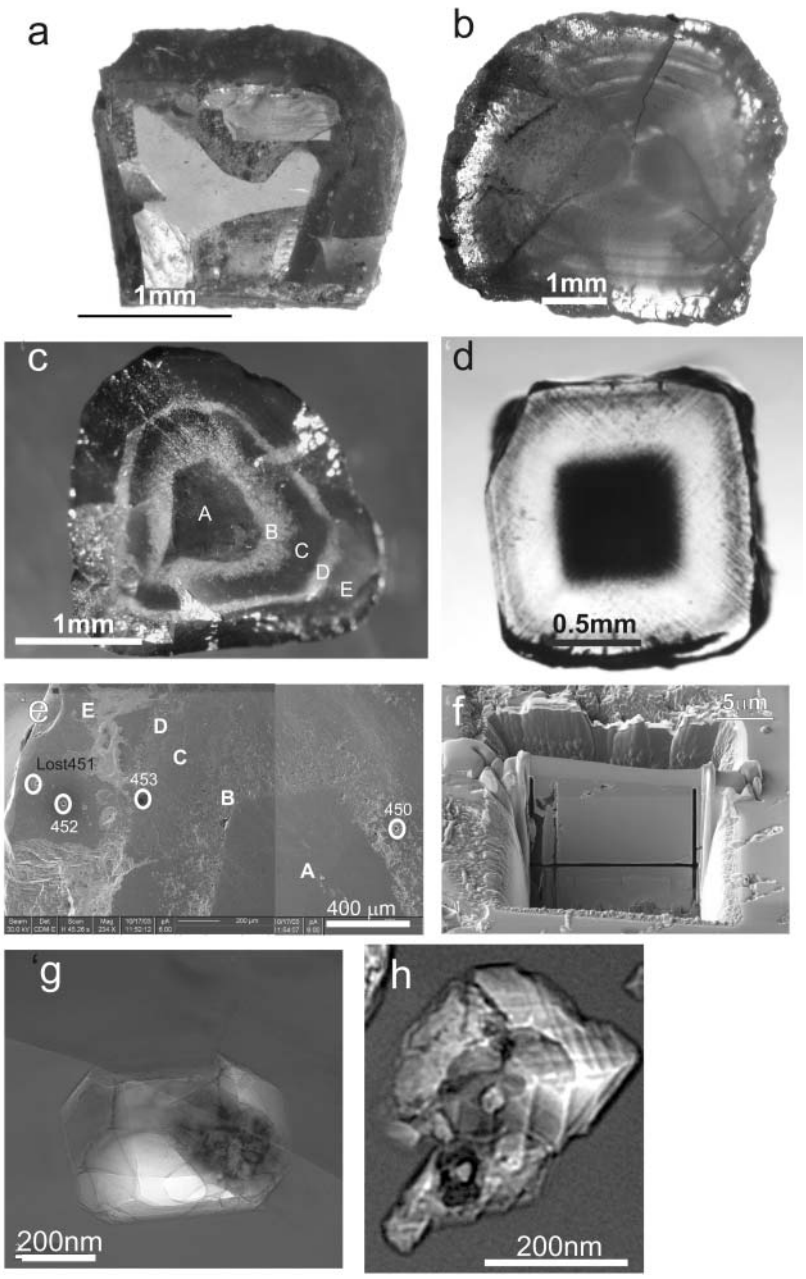

FIGURE 1. Images of diamond sections (**a**–**d**). Transmitted light micrographs of diamond slabs of diamond ON-DVK-272 (**a**), ON-DVK-281 (**b**), ON-DVK-294 (**c**), and UB 5-41 (**d**). The concentric zones in (c) are marked by letters: A-core, B-inner cavity-rich zone, C-inner fibrous zone, D-outer cavity-rich zone, E-outer fibrous zone. (**e**) A focused ion beam (FIB) image showing the location of foils extracted for TEM analysis from diamond ON-DVK-294 (zones A-E as in **c**); (**f**) Diamond foil (10 × 15 × 0.2 µm) just before extraction. The image shows the foil in the center of a rectangular pit milled by the focused ion beam. The foil was later extracted under the microscope using a glass fiber; (**g**) a microinclusion showing cubic and octahedral faces reflecting diamond habit; (**h**) a microinclusion showing carbonate with rhombohedral growth habit, the microinclusion exhibits a multi-phase filling (phlogopite + carbonate).

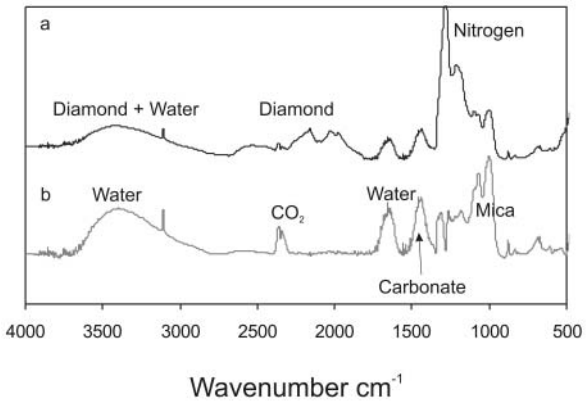

FIGURE 2. FTIR spectra of diamond ON-DVK-281. (**a**) The recorded spectrum that includes intrinsic bands of the diamond matrix (in the two and three phonon regions), absorption due to nitrogen impurities in the diamond matrix (N, mostly type IaA spectrum), and bands due to absorption by the material in the inclusions. (**b**) Residual spectrum after subtraction of standard spectra of the diamond bands and the best-fitted amount of absorption by the various N centers in the diamonds. Note the water bands at 3420 and 1640 cm^{-1} and carbonate bands at 1448 and 880 cm^{-1}. Peaks at 1150–1300 cm^{-1} are mostly remnants from the imperfect subtraction of bands caused by N in the diamond matrix. Mica bands are located between 900 and 1100 cm^{-1} (see Fig. 3 for details). The CO_2 band at 2340 cm^{-1} includes a contribution from atmospheric CO_2.

TABLE 1. Average compositions of the fluid microinclusions as measured by EPMA and IR

Diamond	ON-DVK-272		ON-DVK-281		ON-DVK-294‡				UB 5-41
					Hydrous-saline rich		Carbonatitie melt		Carbonatitie melt
wt%	Average	Std	Average	Std	Average	Std	Average	Std	Average
Number of analyses	21		55		71		61		2
Analytical Total*	3.2	1.3	3.4	1.5	3.9	2.0	5.0	2.3	3.6
SiO_2†	4.3	2.4	27.6	4.0	6.4	2.4	9.3	2.8	7.3
TiO_2	0.2	1.1	2.5	2.3	0.8	1.5	1.0	1.7	1.5
Al_2O_3	0.8	1.2	3.5	1.7	0.9	1.4	1.6	1.3	1.5
FeO	7.4	3.6	12.6	3.4	6.3	3.0	7.7	2.0	9.5
MgO	3.6	1.9	6.1	1.8	9.1	2.4	18.6	2.6	10.6
CaO	7.4	3.1	14.0	3.2	8.1	2.4	13.0	3.1	15.3
BaO	11.7	5.5	2.6	3.7	10.2	4.6	7.7	4.2	1.1
Na_2O	8.5	2.6	3.0	1.7	17.6	4.7	15.5	2.6	12.1
K_2O	28.9	6.5	22.4	3.4	20.0	4.6	13.1	2.0	24.5
P_2O_5	0.3	0.7	3.3	2.2	2.0	1.8	3.0	1.8	6.3
Cl	31.9	3.1	1.8	1.1	21.6	5.1	9.1	2.8	7.8
$CO_2/(H_2O+CO_2)$§	0.21		0.27		No IR Data		No IR Data		0.56
CO_2‖	16.93		42.7						52.12
H_2O#	63.70		115.4						41.41
					Normalized to 100% molar				
Si	3.1	1.7	25.0	3.6	4.6	1.8	7.2	2.2	5.8
Ti	0.1	0.5	1.7	1.6	0.4	0.8	0.6	1.0	0.9
Al	0.6	1.0	3.8	1.8	0.8	1.2	1.4	1.2	1.4
Fe	4.5	2.2	9.6	2.7	3.8	1.9	5.0	1.4	6.3
Mg	3.9	2.1	8.2	2.3	9.8	2.8	21.4	3.0	12.4
Ca	5.7	2.4	13.5	3.0	6.3	2.1	10.7	2.6	13.0
Ba	3.4	1.6	0.9	1.4	2.9	1.4	2.4	1.3	0.4
Na	11.9	3.5	5.2	2.9	24.4	5.1	23.2	3.6	18.5
K	26.4	5.2	25.9	3.7	18.4	3.8	12.9	1.9	24.7
P	0.2	0.4	2.6	1.7	1.2	1.1	2.0	1.2	4.2
Cl	38.9	3.0	2.7	1.8	26.1	4.7	11.9	3.6	10.4

* Total amount of oxides and Cl before normalization (the rest being mainly carbon from the surrounding diamond).
† All components except CO_2 and water are measured by EPMA and are normalized to 100%.
‡ The data for ON-DVK-294 is divided to carbonatitic melt and hydrous-saline rich compositions due to compositional zoning within the diamond (Klein-BenDavid et al. 2004).
§ The $CO_2/(CO_2 + H_2O)$ molar ratio is calculated from the IR spectrum using absorption coefficients of water and carbonates from Navon et al. (1988).
‖ The CO_2 content is calculated based on the assumption that:
CO_2 in carbonate estimated as $CO_3^{2-} = Ca^{2+} + Mg^{2+} + Fe^{2+} + Ba^{2+} + 0.5Na^{+} + 0.5K^{+} - 0.5Cl^{-} - 1.5PO_4^{3-}$.
The H_2O content is calculated fom the CO_2 value and the $CO_2/(CO_2 + H_2O)$ ratio.

ficients of Navon et al. (1988). The $CO_2/(CO_2+H_2O)$ ratio (CO_2 – as inferred from carbonates) is higher in sample UB5-41, in which the composition of the inclusions is closer to that of the carbonatitic end-member (Table 1).

The bulk compositions of the microinclusions were determined using EPMA. Each of the four selected diamonds display distinct compositional ranges that fall within the known range of microinclusions (Fig. 4). The compositions of the microinclusions in diamond ON-DVK-281 fall along the array between the carbonatitic and the hydrous-silicic end-members. Diamond ON-DVK-272 is enriched in the hydrous-saline component; diamond ON-DVK-294 is zoned and spans a wide compositional range between the carbonatitic and hydrous-saline end-members. EPMA analysis of individual microinclusions in diamond UB 5-41 yielded two different compositions: carbonatitic HDF was found in two microinclusions, whereas 15 other microinclusions contained S-Fe-Ni-rich compositions. The foil extracted for TEM analysis contained no sulfide microinclusions, thus the EPMA analysis of the microinclusions carrying sulfide melt are not included in this paper.

Table 1 presents the average compositions of the fluid microinclusions measured in each of the four diamonds. Detailed EPMA analyses of individual microinclusions in diamond ON-DVK-294 and UB 5-41 are presented in Klein-BenDavid et al. (2004) and Logvinova et al. (2003) and Klein-BenDavid et al. (2003b) respectively. Those of the other two diamonds will be discussed elsewhere, together with additional diamonds from Canada (Klein-BenDavid et al. In preparation)

TEM results

General description of the microinclusions. The microinclusions range between 30 and 700 nm in diameter. They are anhedral to euhedral in shape, reflecting the diamond habit (Fig. 1g). Lattice dislocations are found around some microinclusions. These appear as short lines extending from the microinclusion into the diamond matrix; diffraction fringes are bent around these dislocations. All of the microinclusions contain one to several mineral phases and vacant space (commonly less than 40% of the volume). This space was probably filled with a low-density fluid prior to the preparation and extraction of the foil, although in some cases, loss of solid material may also have occurred. In most cases, the vacant spaces do not penetrate the full width of the diamond foil, leaving a thinner diamond matrix (the inclusion wall). This is concluded from the bright contrast visible in bright-field images and from plasmon images that demonstrate that this bright contrast is not due to a hole in the foil.

Diamond ON DVK 272. Seven microinclusions from one foil were analyzed (Table 2). Figure 5 presents six inclusions in a 2.8

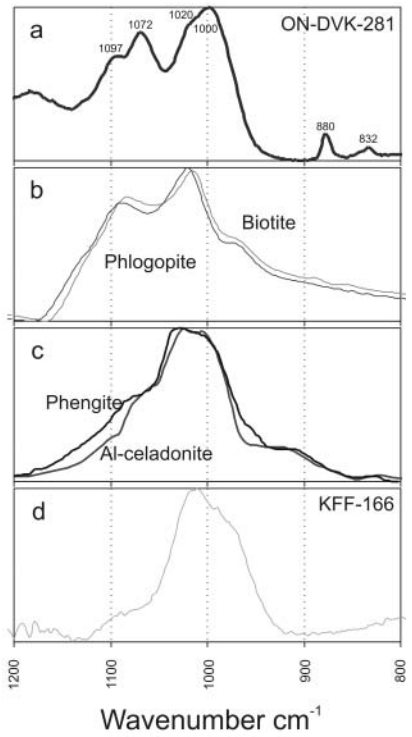

FIGURE 3. FTIR spectra of mica between 800–1200 cm^{-1}. (**a**) Mica-bearing diamond ON-DVK-281. (**b**) Biotite (Name: Biotite $K(MgFe^{+2})_3(ALFe^{+3})Si_3O_{10}(OH,F)_2$ 2002) and phlogopite (Name: Phlogopite $KMg_3Si_3AlO_{10}(F,OH)_2$ 2002) standards. (**c**) Phengite standard (Mookherjee and Redfern 2002) and Al-celadonite (Beran 2002). (**d**) Mica-bearing diamond KFF-166 from Koffiefontein (Izraeli et al. 2004).

× 1.7 μm^2 area in the foil; one (A) is empty. The element maps retrieved by EDAX analysis show that K and Cl are present in all five microinclusions; Ca is abundant in three, and Ba in two. The Ca- and Ba-rich zones do not overlap with the K- and Cl-rich areas, indicating that they reside in different phases. EDS of the solid phases within these inclusions yield compositions that are intermediate between those of KCl and carbonate. This result probably means that the boundary between neighboring crystals is intricate and that the beam penetrates overlying phases.

The halide is composed of K and Cl, with K/Cl~1. No diffraction pattern of the halide phase could be retrieved due to rapid decomposition under the beam. For the Ca-Mg-Fe rich phase, EELS indicates bonding to carbonate ions. IR spectroscopy also indicates the presence of carbonate in this diamond. Most carbonates have molar compositions indicative of ferroan dolomite (50% Ca; 30% Mg and 20% Fe; Fig. 6). Two analyses indicate Mg-Fe-rich carbonate. Ba-rich analyses suggest the presence of Ba-carbonate (e.g., analysis 18 of diamond ON-DVK-272 in Table 2).

Figure 7 shows a line scan across another microinclusion that contains both carbonate and halide phases. The distribution of Ca, Mg, and Fe is not uniform and, at the right-hand side of the scan, Mg and Fe concentrations increase whereas Ca concentration decreases. A slight increase in Si concentration (not shown)

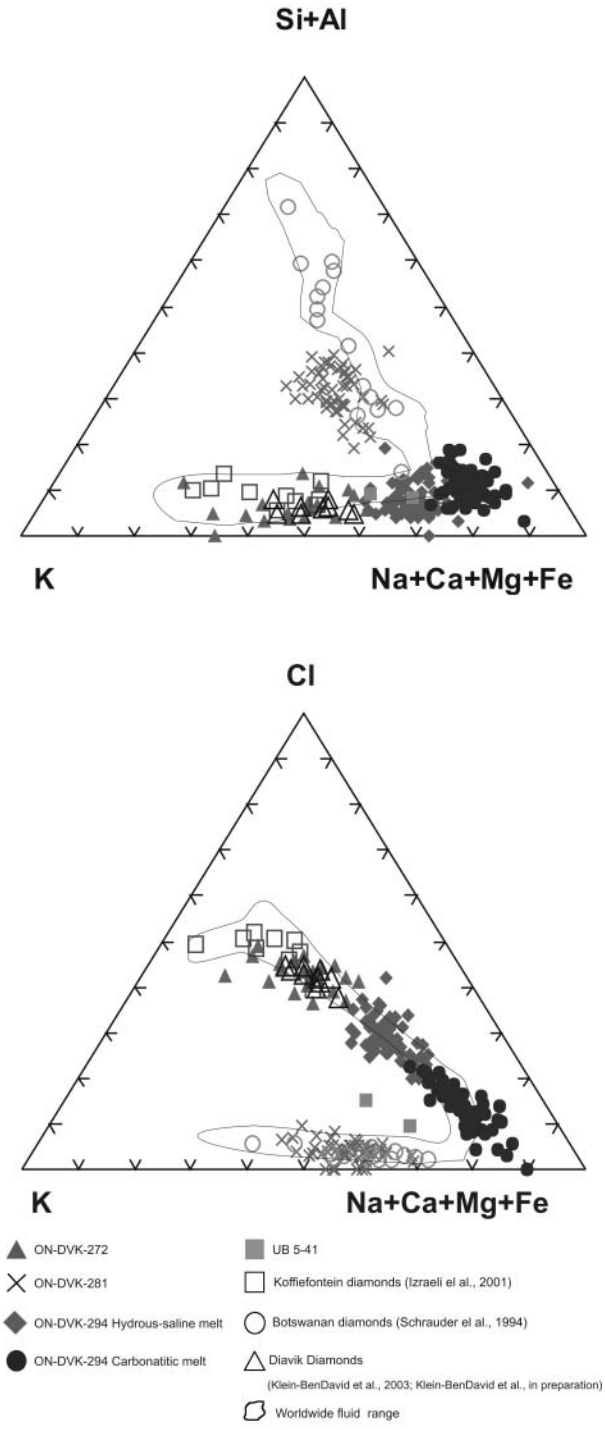

FIGURE 4. Compositions (molar proportions) of all the analyzed microinclusions in all four diamonds as measured by EPMA. Also presented are the average compositions of the inclusions in individual fibrous diamonds from Botswanan (Schrauder and Navon 1994), Diavik Diamonds (Klein-BenDavid et al. 2003a; Klein-BenDavid et al. in preparation) and Koffiefontein cloudy diamonds (Izraeli et al. 2001) and the range they span.

TABLE 2. TEM-EDAX analysis of selected phases identified in the microinclusions in the diamond foils*†

Diamond no.#	ON-DVK-272				ON-DVK-281				ON-DVK-294		ON-DVK-294	
Foil no.†	446				418				453		452	
Phases	Halide + Carbonate	Carbonate + silicate	Ba-Carbonate+ halide + silicate	Carbonate + halide + silicate	High silica mica	Carbonate	Carbonate + mica	Apatite	Halide	Carbonate + apatite + silicate + halide	Carbonate	Pyroxene
Normalized wt%												
Analysis no.†	1	6	18	20	4	6	18	31	23	28	12	28
SiO_2	–	9.7	8.7	6.5	57.1	0.8	18.2	–	–	7.9	3.2	51.7
TiO_2	–	–	–	–	5.2	–	7.8	–	–	–	–	–
Al_2O_3	–	–	–	–	8.7	–	–	–	–	–	–	9.1
FeO	–	17.1	–	15.6	12.0	25.3	11.1	2.8	–	13.6	10.7	9.1
MgO	–	22.3	4.2	11.7	8.1	17.2	–	–	–	13.9	26.3	24.8
CaO	0.4	44.6	–	24.3	–	54.5	55.7	55.3	–	17.1	41.7	–
BaO	5.4	3.5	47.8	23.5	–	–	–	–	–	11.2	2.1	–
K_2O	68.0	2.8	21.9	8.8	8.8	–	7.2	–	65.1	26.3	1.2	2.9
P_2O_5	–	–	–	–	–	–	–	42.0	–	7.8	2.3	2.4
Cl	33.8	–	22.5	12.4	–	–	–	–	45.1	2.7	0.7	–
SO_3	–	–	–	–	–	2.3	–	–	–	–	5.2	–
SrO	–	–	–	–	–	–	–	–	–	–	5.7	–
Normalized to 100% molar												
Si	–	8.8	8.7	6.3	54.6	0.7	17.8	–	–	7.4	3.0	45.9
Ti	–	–	–	–	3.7	–	5.7	–	–	–	–	–
Al	–	–	–	–	9.8	–	–	–	–	–	–	9.5
Fe	–	13.0	–	12.5	9.6	19.7	9.1	2.4	–	10.6	8.3	6.8
Mg	–	30.2	6.3	16.7	11.5	23.9	–	–	–	19.3	36.3	32.8
Ca	0.3	43.4	–	24.9	–	54.4	58.4	61.0	–	17.1	41.3	–
Ba	1.5	1.2	18.8	8.8	–	–	–	–	–	4.1	0.8	–
K	59.2	3.3	28.0	10.8	10.7	–	9.0	–	52.1	31.2	1.4	3.3
P	–	–	–	–	–	–	–	36.6	–	6.2	1.8	1.8
Cl	39.0	–	38.3	20.1	–	–	–	–	47.9	4.2	0.4	–
S	–	–	–	–	–	1.2	–	–	–	–	2.8	–
Sr	–	–	–	–	–	–	–	–	–	–	3.1	–

* Most analyses display mixed compositions of superimposed phases.

† Deposit item AM-06-006, appendix tables. Deposit items are available two ways: For a paper copy contact the Business Office of the Mineralogical Society of America (see inside front cover of recent issue) for price information. For an electronic copy visit the MSA web site at www.minsocam.org, or go to the American Mineralogist Contents, find the table of contents for the specific volume/issue wanted, and then click on the deposit link there.

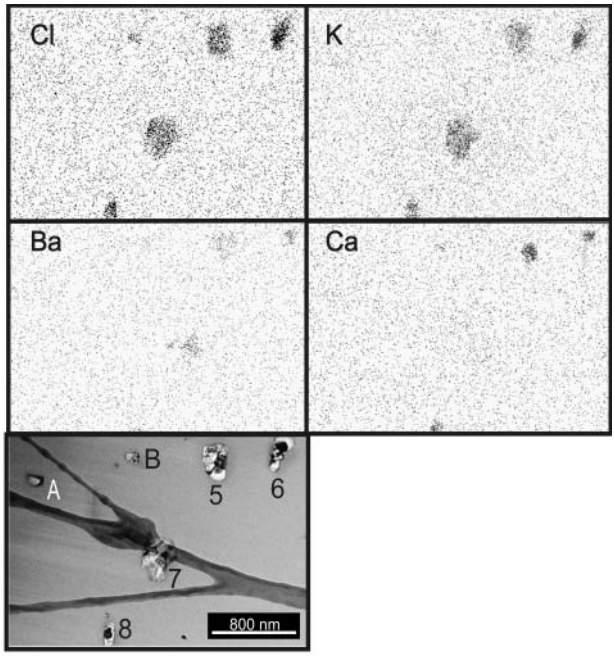

FIGURE 5. Element map of microinclusions in diamond ON-DVK-272 using Cl*K*α, KKα, Ba*L*, and Ca*K*α X-ray intensities. The dark lines in the background are due to the supporting film.

at the right-hand side of the inclusion is too small to account for the large increase in Fe, indicating heterogeneity in the carbonate composition.

The above observations indicate that the carbonate composition is variable both within and among neighboring microinclusions. The diversity among neighboring microinclusions may be the result of: (1) entrapment of a heterogeneous HDF; (2) necking of a large inclusion after cooling and crystallization; and (3) material loss during sample preparation. As no evidence for necking was observed and as bulk microinclusion composition measured by the EPMA is relatively homogeneous, we suggest that the microinclusions were penetrated during FIB milling and that some of their original content lost. It is also possible that some variability is due to the original entrapment of HDF + minute crystals (cf., Izraeli et al. 2004).

Diamond ON DVK 281. One FIB foil was cut from diamond ON-DVK-281, and five microinclusions were detected. The microinclusions in this diamond are relatively homogenous in composition and contain several distinguishable crystalline phases. A Ca-Mg-Fe carbonate phase was identified in four of the microinclusions (Fig. 6). It contains on average 55% Ca, 22.5% Fe, and 22.5% Mg (molar proportions) and minor amounts of Ba. In two microinclusions, a Ca- and P-rich phase was detected with lattice fringe spacings that fit that of apatite (Table 3).

A K-rich phase, with a composition that corresponds to that of high-silica mica, was detected in all of the microinclusions. The lattice fringe spacings presented in Table 3 correspond to those of micas. The Si content of the mica is on average 7.4 ± 0.3 Si atoms per formula unit (pfu, for 22 O atoms), much higher than the 6 atoms in common biotite or phlogopite. The Al cation proportion of the high-silica mica is low, 1.2 ± 0.3 pfu, but because of the high Si content, only ~0.6 Al pfu is needed to complete the

TABLE 2. — *Extended*

ON-DVK-294 450				UB 5-41 455			
Si-rich phase	Al-rich phase	Ca-rich phase	Element map	Si-rich phase	Al-rich phase	Ca-rich phase	Element map
37	48	47	12	14	18		
55.3	3.9	0.6	34.7	94.7	3.5	2.5	14.9
–	–	–	–	–	–	–	2.3
26.4	94.8	1.3	29.2	5.3	93.5	7.0	69.1
7.6	0.5	0.6	6.9	–	1.6	1.6	1.9
–	–	0.9	5.5	–	–	–	–
6.7	0.6	94.4	15.8	–	0.9	88.2	9.8
–	–	–	–	–	–	–	–
1.9	0.3	1.0	2.5	–	–	–	1.1
2.2	–	–	3.8	–	–	–	–
–	–	–	0.3	–	0.8	0.8	1.3
–	–	–	1.4	–	–	–	–
–	–	1.1	–	–	–	–	–
53.1	3.3	0.6	32.3	93.8	2.9	2.4	13.1
–	–	–	–	–	–	–	1.5
29.9	95.5	1.5	32.0	6.2	94.0	7.7	71.6
6.1	0.3	0.4	5.4	–	1.1	1.3	1.4
–	–	1.3	7.6	–	–	–	–
6.9	0.5	94.4	15.8	–	0.8	87.4	9.2
–	–	–	–	–	–	–	–
2.3	0.3	1.2	3.0	–	–	–	1.2
1.8	–	–	3.0	–	–	–	–
–	–	–	0.2	–	1.1	1.3	1.9
–	–	–	0.8	–	–	–	–
–	–	0.6	–	–	–	–	–

* Most analyses display mixed compositions of superimposed phases.

tetrahedral occupancy, leaving ~0.6 Al pfu in octahedral sites. Together with Mg, Fe, and minor Ti, the octahedral sites are occupied by 4.7 ± 1.1 cations pfu. The average Mg no. of the mica is 0.53 ± 0.06. The K cation content is 1.8 ± 0.3 pfu (Table 4). In the discussion, we conclude that this mica is intermediate between phlogopite-biotite and Al-celadonite.

Diamond ON DVK 294. The microinclusions in diamond ON-DVK-294 span a wide compositional range between the carbonatitic and the hydrous-saline end-members. The hydrous-saline-enriched microinclusions are located in the inner fibrous zones (C and E in Fig. 1c), and the carbonatitic component is enriched in the microinclusions of the outer fibrous zone (the outer part of E in Fig. 1c). Cavities up to 20 μm in size were observed in zones B and D (Fig. 1c, Klein BenDavid et al. 2004). Three FIB foils were cut from the different zones of the diamond (Fig. 1e): two from the inner and outer fibrous layers and one from a cavity-rich zone. Each foil exposed different features and will be discussed separately.

Foil 452 was cut from the outer fibrous zone (E in Figs. 1c and 1e). In contrast to the relatively homogenous chemical composition in the microinclusions of the previous diamond, the five microinclusions in this foil differ. EDAX analyses (Fig. 6) recorded carbonate, silicate, and apatite. Carbonate composition spans the range between Mg-Ca carbonate with minor Sr, Ba, and Fe, and Mg carbonate with about 15% Fe. The silicate is rich in Si, Mg, Fe, and Al but also carries small amounts of K and P. Assuming that K and P reside in accessory phases, its formula is $Mg_{1.52}Fe_{0.31}Al_{0.34}Si_{1.83}O_6$, similar to that of a pyroxene with Mg no. = of 0.83.

All the microinclusions contain one or more of these phases.

TABLE 3. Diffraction data of apatite and high-silica mica in five microinclusions in foil 418 of diamond ON-DVK-281

Mineralogy	d *hkl* observed (Å)	*hkl*	d *hkl* calculated (Å)
Apatite	3.65	(0002)	3.44
Apatite	4.18	(2020)	4.06
	6.48	(0001)	6.88
High-silica mica	4.78	(020)	4.6
	3.29	(11$\bar{2}$)	3.15
		(02$\bar{2}$)	3.4
High-silica mica	4.56	(110)	4.54
		(020)	4.6
High-silica mica	3.52	(02$\bar{2}$)	3.4
	3.72	($\bar{1}$12)	3.67
	4.56	($\bar{1}$10)	4.54
High-silica mica	3.65	(112)	3.67
High-silica mica	1.09	(001)	1.01

An example of this multiphase nature of the microinclusions in this sample is presented in Figure 8. The microinclusion is dominated by Ca- and Mg-rich carbonates. Apatite is detected left of the microinclusion center and an Mg-silicate occurs on its right side.

Foil 453 was cut from the inner fibrous zone (C in Figs. 1c and 1e). Seven microinclusions were detected. Their compositions vary between K-Cl-rich and Ca-Mg-Fe-rich (Fig. 6). Carbonates span a similar range to those analyzed in foil 452. Minor amounts of Si are also present.

The K/Cl ratio of the halide phases in three of the microinclusions is about 1. Sodium was not measured, but its presence is confirmed by EPMA analyses of microinclusions in this zone. As Cl is compensated by K, the Na is most probably bound in carbonate. A phase having a lower K/Cl ratio of 0.43 ± 0.4 in one of the microinclusion is interpreted as Na-K-halide. An analysis yielding a high K/Cl ratio (5.4 ± 1.2) in another microinclusion is attributed to the presence of a non-halide K-bearing phase. As the Si concentration in this microinclusion is low and it contains mainly carbonate, it is likely that the K is bound in a carbonate phase.

Foil 450 was cut from the inner cavity-rich zone (B in Figs. 1c and 1e). The foil exposes two elongated cavities that are much larger than the typical microinclusions: 1 × 4 μm^2 and 2.5 × 8 μm^2. The cavities contain both filled and empty volumes. Two microinclusions that resemble those described previously were detected near the cavities (Fig. 9). Microinclusion 1 contains Mg-Ca-Fe carbonate, Si-K-rich component, and minor K-Cl-rich halide. Microinclusion 2 contains mainly apatite and Ba-rich carbonate. Minor Si, K, and Cl were also detected.

The material in the cavities is completely different from that of the microinclusions. Most of the material in both cavities is amorphous, with only a few small crystals detected within the bulk amorphous matrix. The composition of this matrix differs from that of the fluids commonly found in diamond microinclusions. Cavity 1 is rich in Al and has lesser Si. Cavity 2 is more heterogeneous and is filled with three distinct amorphous phases (Fig. 10). The dominant phase is rich in Al, with a few other elements. An Si-rich phase also contains Al, Mg, Fe, and K. A Ca-rich phase also contains minor P. Figure 6d displays the compositional range observed in the two areas.

Diamond UB 5-41. One FIB foil was cut from diamond UB 5-41. Three cavities (3.0, 0.68, and 0.75 μm in size) were exposed. We investigated the large cavity, which is filled with

TABLE 4. Compositions of high-silica mica as measured in five microinclusions in foil 418 of diamond ON-DVK-281

	Inclusion 1							Inclusion 2									Inclusion 3					
Wt%	1	2	3	4	5	Average	std	15	16	17	21	22	23	24	Average	std	25	26	27	28	29	Average
SiO_2	57.1	57.7	57.5	57.1	58.1	57.5	0.42	51.4	50.8	48.4	49.7	48.5	50.6	50.2	49.9	1.15	54.6	55.7	52.4	55.1	51.4	53.8
TiO_2	5.6	6.2	5.7	5.2	5.0	5.5	0.47	5.4	5.8	5.4	4.9	5.6	5.2	5.9	5.5	0.35	7.7	5.9	6.3	6.2	6.1	6.4
Al_2O_3	7.2	8.5	8.0	8.7	8.6	8.2	0.62	6.3	7.7	7.8	7.0	5.6	7.5	7.3	7.0	0.81	–	8.5	7.3	7.1	9.2	6.4
FeO	12.8	11.8	11.3	12.0	11.1	11.8	0.67	16.5	16.6	16.8	15.9	17.4	14.7	15.4	16.2	0.92	15.7	14.4	14.6	13.1	14.1	14.4
MgO	7.8	6.9	9.4	8.1	9.3	8.3	1.06	10.4	11.0	11.2	12.3	11.8	11.0	9.9	11.1	0.81	9.1	4.4	8.0	7.6	6.1	7.0
CaO	–	–	–	–	–	–	–	–	–	–	1.1	3.3	0.6	1.25	–	–	–	–	–	–	–	–
K_2O	9.2	8.5	7.6	8.8	7.9	8.4	0.65	10.1	8.0	10.4	10.1	11.1	9.9	8.1	9.7	1.17	13.0	11.0	11.4	10.9	13.0	11.9
Cl	0.4	0.4	0.3	–	–	0.2	0.21	–	–	–	–	–	–	–	–	–	–	–	–	–	–	–
Total	100	100	100	100	100			100	100	100	100	100	100	100			100	100	100	100	100	
Formula proportions based on 22 O atoms																						
Si	7.7	7.7	7.6	7.6	7.6	7.6	0.03	7.2	7.0	6.8	7.0	6.9	7.0	7.0	7.0	0.11	7.7	7.6	7.3	7.5	7.2	7.5
Ti	0.6	0.6	0.6	0.5	0.5	0.6	0.05	0.6	0.6	0.6	0.5	0.6	0.5	0.6	0.6	0.04	0.8	0.6	0.7	0.6	0.6	0.7
Al	1.1	1.3	1.2	1.4	1.3	1.3	0.09	1.0	1.3	1.3	1.2	0.9	1.2	1.2	1.2	0.13	–	1.4	1.2	1.1	1.5	1.0
Fe	1.4	1.3	1.3	1.3	1.2	1.3	0.08	1.9	1.9	2.0	1.9	2.1	1.7	1.8	1.9	0.12	1.9	1.6	1.7	1.5	1.6	1.7
Mg	1.6	1.4	1.9	1.6	1.8	1.6	0.20	2.2	2.3	2.4	2.6	2.5	2.3	2.0	2.3	0.18	1.9	0.9	1.7	1.5	1.3	1.5
Ca	–	–	–	–	–	0.0	0.00	–	–	–	–	–	0.2	0.5	0.1	0.19	–	–	–	–	–	0.0
K	1.6	1.4	1.3	1.5	1.3	1.4	0.12	1.8	1.4	1.9	1.8	2.0	1.8	1.4	1.7	0.22	2.3	1.9	2.0	1.9	2.3	2.1
Cl	0.1	0.1	0.1	–	–	0.0	0.04	–	–	–	–	–	–	–	0.0	0.00	–	–	–	–	–	0.0

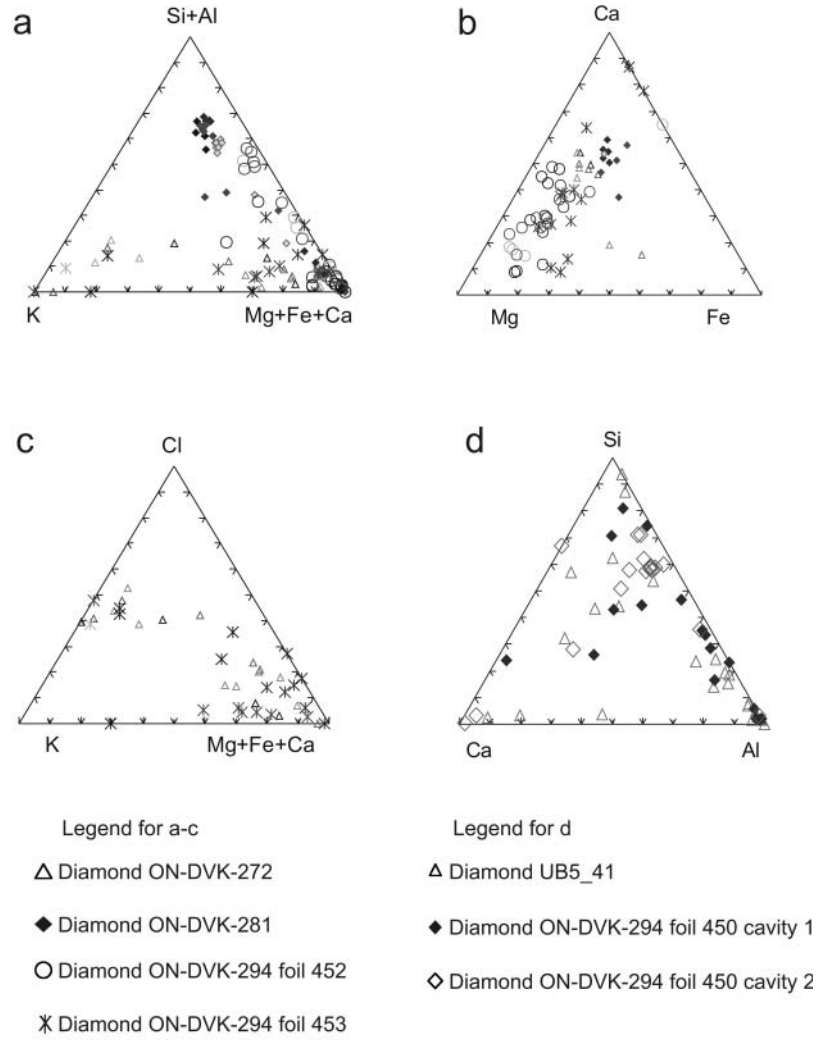

FIGURE 6. Compositions of solid phases in microinclusions measured by TEM-EDAX (all in molar proportions). (**a**) All microinclusions presented on a Si + Al, Mg + Fe + Ca, and K ternary diagram. (**b**) Carbonate-bearing microinclusions presented on a Mg, Ca, and Fe ternary diagram. (**c**) Halide-bearing microinclusions presented on a Cl, Mg + Fe + Ca, and K ternary diagram. (**d**) Cavity-fill composition presented on a Si, Al, and Ca ternary diagram.

three phases: Al-rich, Ca-rich, and Si-rich; part of the cavity is now empty. Diffraction patterns and dark-field images indicate that most of the matrix is amorphous; small crystals (10–200 nm) of various minerals were detected within the bulk amorphous matrix. EELS indicated that Al is bonded to O and Ca is bonded to CO_3. The Si-rich phase also contains Fe, K, and Cl. The concentrations of the latter two correlate positively.

DISCUSSION

Microinclusion fillings

TEM imaging and analysis of FIB-milled foils provide unique observations into microinclusions in diamonds. TEM imaging of the microinclusions detected multiphase mineral assemblages. In most cases, vacant spaces were also present in the microinclusions and were probably filled with low-density fluids before the microinclusions were exposed during sample preparation. This conclusion is supported by the following observations: Guthrie et al. (1991) reported an amorphous phase that moved under the beam and interpreted it as a fluid phase. IR spectra of the diamonds show abundant water in the microinclusions. Navon (1991) showed that the microinclusions in diamonds from Zaire are under high internal pressure (1.5–2 GPa at room temperature) and attributed it to a compressed volatile phase. Last, high K concentrations that cannot be accommodated by mica and halides were found in the microinclusions. This excess K (Fig. 11) is probably concentrated in the low-density residual fluid that was lost

TABLE 4. — *Extended*

Inclusion 4						Inclusion 5				
std	32	33	34	35	40	Average	std	42	Average All	Stdev
1.85	55.8	56.1	56.4	56.7	53.7	55.7	1.19	43.6	53.4	3.8
0.72	6.8	5.2	5.4	5.3	7.0	5.9	0.88	1.2	5.6	1.2
3.69	7.6	8.3	8.3	6.8	7.3	7.7	0.65	8.8	7.4	1.8
0.94	12.1	11.6	11.6	13.6	12.8	12.3	0.86	20.3	14.2	2.4
1.83	8.2	8.4	8.8	6.5	8.3	8.0	0.89	11.3	8.9	2.0
–	–	–	0.2	0.7						
1.06	9.6	10.4	9.5	11.0	10.9	10.3	0.71	14.7	10.2	1.8
–	–	–	0.0	0.1						
	100	100	100	100	100			100		
0.23	7.5	7.5	7.5	7.7	7.3	7.5	0.14	7.3	7.4	0.3
0.08	0.7	0.5	0.5	0.5	0.7	0.6	0.09	0.1	0.6	0.1
0.60	1.2	1.3	1.3	1.1	1.2	1.2	0.09	1.5	1.2	0.3
0.13	1.4	1.3	1.3	1.6	1.5	1.4	0.11	1.7	1.6	0.3
0.39	1.6	1.7	1.8	1.3	1.7	1.6	0.17	2.2	1.8	0.4
0.00	–	–	–	–	–	0.0	0.00	–	0.0	0.1
0.22	1.6	1.8	1.6	1.9	1.9	1.8	0.14	1.8	1.8	0.3
0.00	–	–	–	–	–	0.0	0.00	–	0.0	0.0

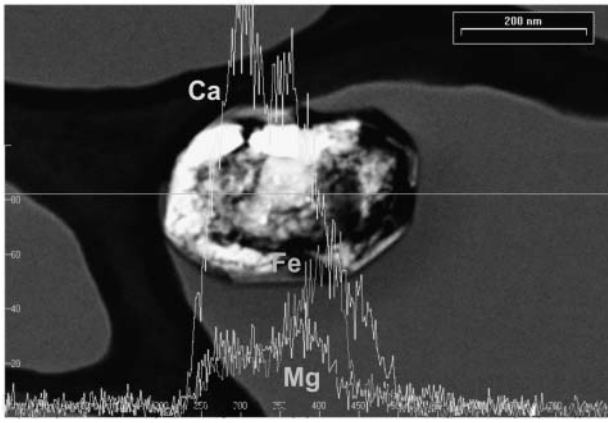

FIGURE 7. Scanning TEM image with line-scan across a microinclusion in diamond ON-DVK-272 showing Ca$K\alpha$, Fe$K\alpha$, and Mg$K\alpha$ X-ray intensities. The dark areas in the background are the perforated carbon film supporting the foil.

during foil preparation. The high volatile fraction of secondary solids suggests that the material trapped in the inclusions was a melt-like, high-density, supercritical fluid. Upon cooling, this fluid was quenched to solid phases and a residual low-density, water-rich fluid.

Microinclusion heterogeneity

Although EPMA of microinclusions from the same diamonds display relatively homogenous compositions, some heterogeneity was observed among microinclusions from the same foil. Neighboring microinclusions may contain different mineral phases or show different compositions. Most of the observed variation is attributed to rupture of microinclusion during milling. However, some variation can arise from the entrapment of high-density fluid carrying small crystals that precipitated from it prior to entrapment.

Carbonate minerals

The presence of carbonate minerals in diamond microinclusions was inferred from diffraction patterns (Guthrie et al. 1991;

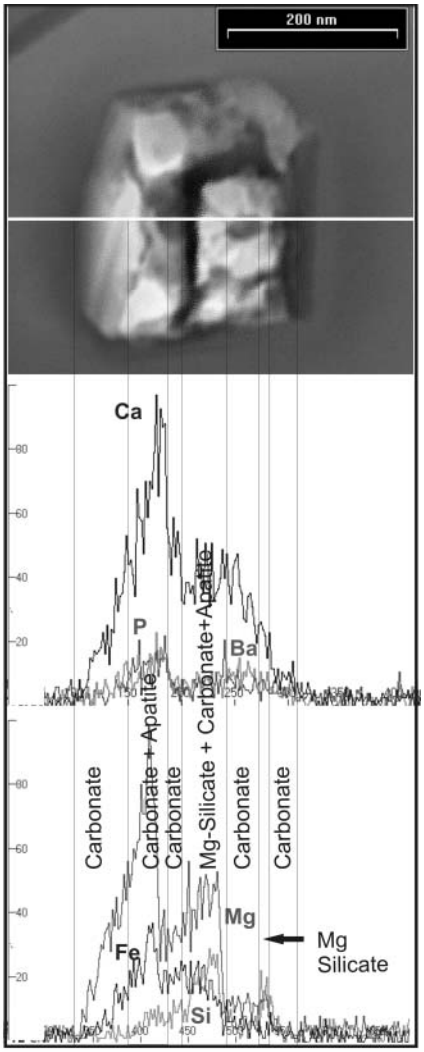

FIGURE 8. Line-scan across a microinclusion in diamond ON-DVK-294 foil 452, illustrating the multi-phase nature of the microinclusion.

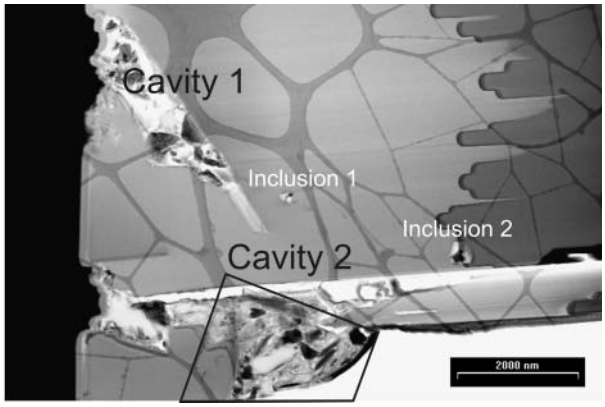

FIGURE 9. Cavities in foil 450 (diamond ON-DVK-294). The frame at the bottom center defines the area of the element map presented in Figure 10. Dark gray horizontal columnar contrasts at the right side of the image are FIB thinning artifacts. The dark lines in the background are part of the supporting carbon film.

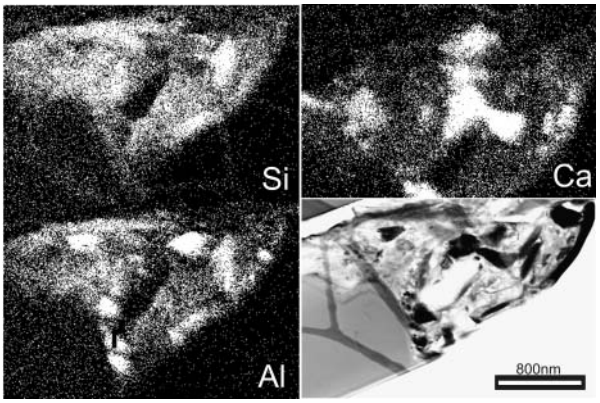

FIGURE 10. Element map of cavity 2 (see Fig. 9). Note the different distribution of the Ca*K*α, Si*K*α, and Al*K*α X-ray intensities.

Walmsley and Lang 1992a), IR spectra of microinclusion bearing diamonds (Chrenko et al. 1967; Navon et al. 1988) and EPMA analysis that detected high Ca, Mg, and Fe with no compensating anions (Schrauder and Navon 1994; Izraeli et al. 2001). The abundance of these elements correlates positively with the $CO_2/(H_2O + CO_2)$ ratio retrieved from the IR spectra (Schrauder and Navon 1994; Izraeli et al. 2001). In the present work, we contribute additional evidence for the presence of carbonates. EELS reveals carbon-K and oxygen-K edges that display the characteristic signatures of carbonates. In addition, we observed some crystals with a rhombohedral habit, characteristic of Mg-Fe carbonates (Fig. 1h).

Carbonate minerals were identified in foils from all diamonds in which microinclusions were studied. They appear in all assemblages, with either halides or silicates, thus emphasizing the

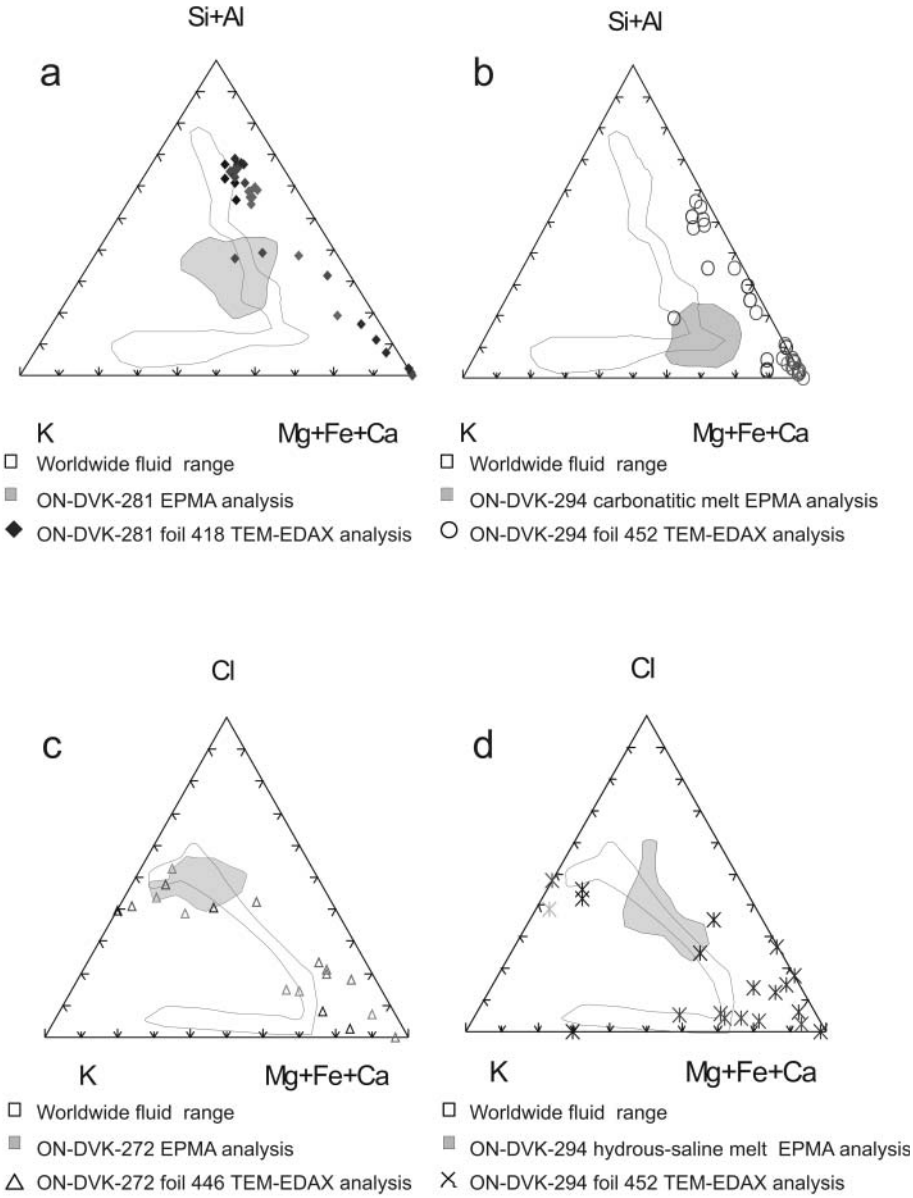

FIGURE 11. TEM-EDAX analyses of phases in the microinclusions (molar proportions). (**a**) diamond ON-DVK-281. (**b**) Foil 452 of diamond ON-DVK-294. (**c**) Diamond ON-DVK-272. (**d**) Foil 453 of diamond ON-DVK-294. Shaded areas: EPMA analyses of the relevant diamonds; open areas – compositional range of diamond from Botswana, South Africa and Canada (See also Fig. 4) (Schrauder and Navon 1994; Izraeli et al. 2001; Klein-BenDavid et al. 2003a; Klein-BenDavid et al. in preparation).

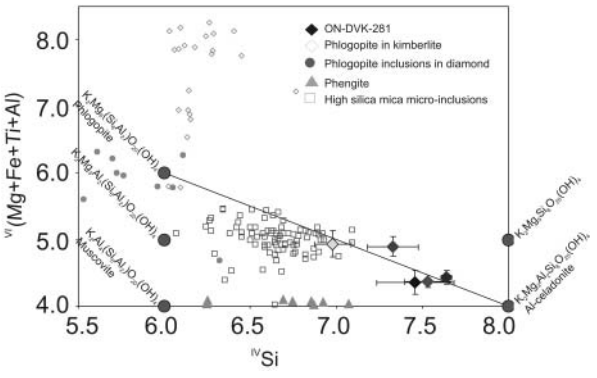

FIGURE 12. A plot of ^{VI}(Mg + Fe + Ti + Al) vs. ^{IV}Si in analyzed micas in the microinclusions of diamond ON-DVK-281 (calculated based on 22 O atoms per formula unit, different shades correspond to the different microinclusions). Also shown: high-silica mica in microinclusions in a diamond from South-Africa (Izraeli et al. 2004); phlogopites in kimberlites (Mitchell 1995b); phlogopite inclusions in diamonds (Giardini et al. 1974; Prinz et al. 1975; Gurney et al. 1979; Meyer and McCallum 1986; Sobolev et al. 1997); and phengites from metamorphic rocks (Hermann 2003; Willner et al. 2004).

importance of carbonatitic HDF in the growth of diamond and the evolution of mantle fluids.

The carbonates identified in diamonds ON-DVK-281 and 272 (Fig. 6b) are ferroan dolomites similar to the high-Ca carbonate identified in microinclusions from Zaire (Guthrie et al. 1991; Walmsley and Lang 1992a). Two of the carbonate analyses in diamond ON-DVK-272 are depleted in Ca and are similar to the low-Ca carbonates reported by Guthrie et al. (1991). Those in ON-DVK-294 are depleted in Fe and span a continuous range between dolomite and magnesite. They resemble the composition of magnesite and dolomite of larger diamond inclusions (Meyer 1987; Harris 1992).

Apatite

Apatite was identified in diamond ON-DVK-281, based on its composition and diffraction pattern. It was identified earlier in microinclusions in diamonds from an unknown source (Lang and Walmsley 1983) and from Zaire (Guthrie et al. 1991). In the Zairian diamond, the apatite coexisted with carbonate and an unidentified sheet silicate. A similar assemblage was identified in diamond ON-DVK-281. Evidence of apatite intergrowth with carbonates is shown in foil 452 of diamond ON-DVK-294 (Fig. 8). No apatite was detected in the hydrous-saline-rich ON-DVK-272.

High-silica mica

High-silica mica was identified in all analyzed microinclusions in diamond ON-DVK-281. The electron diffraction and lattice fringe spacings identified the phase as mica. The silica-rich composition of the mica in diamond ON-DVK-281 deviates significantly from that of phlogopite in diamond inclusions (Meyer 1987; Harris 1992; Sobolev et al. 1997), kimberlites and lamproites (Mitchell 1995a, 1995b). Silicon occupies between 6.8 and 7.7 of the 8 tetrahedral sites with an average of 7.4 ± 0.3 (22 O atoms pfu). Mica in diamond microinclusions also was found by Guthrie et al. (1991) and Walmsley and Lang (1992b), who confirmed elevated Si concentrations but provided no accurate analyses. Izraeli et al. (2004) found high silica mica in microinclusions in cloudy diamonds from Koffiefontein; in these, the Si content is 6.3–7.0 pfu, lower than the present results, but still higher than in phlogopite or biotite (Fig. 12). Mica inclusions containing up to 7.2 Si atoms pfu were recorded in ultrahigh-pressure metamorphic microdiamonds from the Kokchetav massif (Shatsky et al. 1995).

The octahedral sites are occupied by Fe and Mg together with Ti and the non-tetrahedral Al. The occupancy of the octahedral sites range between 4.3 and 4.9 pfu, intermediate between di- and tri-octahedral micas. Octahedral occupancy correlates negatively with Si and falls along the array between Al-celadonite [$K_2Mg_2Al_2Si_8O_{20}(OH)_4$] and phlogopite/biotite [$K_2(MgFe)_6(Si_6Al_2)O_{20}(OH)_4$] (Fig. 12). The average K content is 1.8 ± 0.3 atoms pfu. The relatively low occupancy of the interlayer site can be the result of substitution of Na for K. Alternatively, the low occupancy may compensate for the charge increase in the tetrahedral site, similar to illite-muscovite or talc-phlogopite substitutions.

The IR spectrum of the microinclusions reveals clear mica bands at 460, 832, 1000, 1020, 1072, and 1095 cm^{-1} (Fig. 3a). The locations of the bands show similarities to both phlogopite-biotite and Al-celadonite-phengite (Figs. 3b and 3c). A band at ~1020 cm^{-1} is common to all spectra. The bands at 1000 and 1072 cm^{-1} are close to those of high silica micas (1005 and 1075 cm^{-1}); that at 1095 cm^{-1} is close to the 1090 cm^{-1} band of phlogopite. The phlogopite band at 972 cm^{-1} is missing in the spectrum of ON-DVK-281.

Izraeli et al. (2004) reported IR spectra of high silica mica-bearing diamonds from Koffiefontein (Fig. 3d). In the Koffiefontein spectrum, the 1020 cm^{-1} band is more pronounced then the 1000 cm^{-1} band and an additional band appears at 971 cm^{-1}. The higher intensities of the 1020 and 971 cm^{-1} bands are in agreement with the higher proportion of the phlogopite component relative to the Al-celadonite component in the Koffiefontein microinclusions (Fig. 12).

The mica compositions detected in ON-DVK-281 have not been reported previously. Phlogopite inclusions in diamonds are close to stoichiometric, and may even show Si deficiency (Fig. 12). Some kimberlitic phlogopites show modest Si enrichment above 6 Si atoms pfu (Mitchell 1995b). However, they are depleted in Al and enriched in Fe (tetra-ferri mica substitution). A single analysis of extreme Si-enrichment in such micas was reported by Seifert and Schreyer (1971). Phengites from high-pressure metamorphic rocks have elevated amounts of Si (Guidotti 1984). However, their octahedral sites contain four Al atoms pfu with only trace amounts of divalent ions (Fig. 12).

Schreyer (1965) investigated synthetic Si-rich micas that incorporated both Mg and Al in equal proportions at their octahedral site. He speculated that the immiscibility range between di- and tri-octahedral micas closes at high pressure. The high silica micas in diamond ON-DVK-281 along with the high silica micas described by Izraeli et al. (2004) fall within this range and suggest that the miscibility gap closes under natural conditions at the high pressure of the diamond stability field.

High silica mica included in diamonds was found both as a secondary phase that precipitated from the trapped fluids (this

study) and as a trapped crystalline mineral phase (Izraeli et al. 2004) that was present during the precipitation of the diamonds. This rare occurrence reflects the unique environment where HDF rich in Si, K, and H_2O are present at such high pressure.

Halide

K-Cl rich phases that decomposed rapidly under the beam were detected in diamonds ON-DVK-272 and ON-DVK-294 (foil 453), and are most probably halides. As Na was not analyzed, it is impossible to state the specific halide composition. But, a KCl-dominated halide is most likely as K correlates positively with Cl and the K/Cl ratio is around one. The fact that the K/Cl ratio measured by EPMA for bulk microinclusions from these diamonds is lower then unity suggests that some of the Cl is associated with other ions. Surprisingly, no clear indication for halite was found in this study. The excess Cl is high, and the minor P found in the halide-bearing microinclusions precludes Cl accommodation in apatite. It is possible that the excess Cl resides in the residual fluid released during sample preparation.

Pyroxene

The presumed pyroxene in diamond ON-DVK-294 differs from common orthopyroxene mineral inclusions in diamond by its lower Mg no. (0.83) and high Mg-Tschermak component (10%). The microinclusion contained only pyroxene; thus, it may have been trapped as a primary mineral inclusion. Diopside, chromite, and possible olivine were detected in ON-DVK-294 using EPMA (Klein-BenDavid et al. 2004). However, unlike the present pyroxene, the X_{Mg} of the diopside (0.94) and the olivine (0.93) fall within the common range of diamond inclusions. If the pyroxene is secondary and grew from the fluid, it is the first report of this mineral in the assemblage of secondary phases in diamond fluid microinclusions.

Correlations between TEM, EPMA, and IR results

TEM analyzes the secondary phases within a single microinclusion, EPMA analyzes the bulk composition of individual microinclusions, and IR records the composition of many microinclusions in a certain volume of the diamond. It is significant that the results obtained by all three analytical methods agree with each other and exhibit a coherent set of results. Figure 11 compares the EPMA and TEM data. EPMA analyses show that the bulk compositions of the microinclusions in each diamond span a relatively narrow range. In many cases, this range may be accounted for by the combined chemistry of the solid phases of that diamond as detected using TEM. Where this is not possible (e.g., ON-DVK-281 and foil 294-452), the missing ingredient is K, which may have remained in the residual low-density fluid that filled the vacant part of the microinclusion before it was exposed (cf., Hwang et al. 2005). This assumption is supported by the experimental results of Stalder et al. (2002), who equilibrated fluid and melt with mantle minerals at elevated pressures and temperatures and found that K remained in the residual hydrous solution of the quenched products.

Schrauder and Navon (1994) and Izraeli et al. (2001) have shown a positive correlation between the $CO_2/(CO_2 + H_2O)$ ratios calculated from the infrared spectra and the divalent ion content as detected by EPMA. Here, we note a low $CO_2/(CO_2 + H_2O)$ ratio in diamonds ON-DVK-272 and ON-DVK-281 that carry abundant halides or micas. This ratio is high in diamond UB 5-41, where carbonate phases are more abounded.

Cavity fill

Cavities that are a few micrometers in size were observed in two diamonds: ON-DVK-294 and UB 5-41. The chemical composition of their trapped material is similar. It differs from that of the sub-micrometer inclusions in the same diamonds and is dominated by Al-rich and Si-rich amorphous phases (Fig. 10). To the best of our knowledge, this is the first observation of such compositions within a diamond.

The cavities may be the result of diamond dissolution, but as the cavity-rich zones reside in the inner part of the diamond (Fig. 1e), such dissolution and entrapment of material should have occurred in the diamond stability field. The cavities may have trapped crystalline phases that later became amorphous, e.g., during ascent. Such Al- or Si-rich minerals may evolve during metasomatism of mantle silicates by carbonate and water-rich fluids. Alternatively, the coexistence of the three well-separated, amorphous phases may indicate the entrapment of a homogenous melt that separated immiscibly upon cooling.

Comparison with other diamond microinclusions

The secondary mineral assemblages identified in the microinclusions are broadly similar to those detected at other localities (Lang and Walmsley 1983; Guthrie et al. 1991; Walmsley and Lang 1992a, 1992b). The finding of halides in hydrous-saline-rich microinclusions and pyroxene in a carbonatitic fluid and the full characterization of the high-silica mica add new phases to the suite of secondary minerals in diamond microinclusions. Quartz was reported by Guthrie et al. (1991) in microinclusions with highly silicic composition. No quartz was observed in the diamonds we studied, probably because none was rich enough in silica.

The secondary minerals that crystallized from the trapped fluids differ substantially from primary mineral inclusions in diamonds. Carbonates, phosphates, halides, sheet silicates, and quartz are all rare in the mantle and appear in low abundance, if at all, as macro-mineral inclusions in diamonds.

The presence of this unique assemblage in microinclusions reflects the entrapment of a primary HDF enriched in incompatible elements (Cl, K, P, Ba, and Sr), water, and carbonate under high internal pressure. Entrapment in the diamond ensures high CO_2 pressure that persists in the microinclusions even after ascent to the surface [1.5–2 GPa at room temperature (Navon 1999)]. This high CO_2 pressure ensures bonding of most Mg, Fe, and Ca in stable carbonates and allows for the presence of quartz as reported by Guthrie et al. (1991). The high pressure and the high activity of silica and K_2O also explain the formation of high-silica mica rather than phlogopite that is preferred in the Mg-rich mantle environment. The high content of P leads to precipitation of apatite; the excess K ends up in the residual low-density fluid.

The detection, for the first time, of halides along with carbonates in the chlorine-rich microinclusions strengthens the evidence for the growth of diamonds from chlorine-carbonate-rich fluids.

Carbonate phases were identified in most of the microinclusions, both in silicate assemblages and in saline ones. Carbonatitic compositions are also the link between the two compositional arrays defined by the average compositions detected using EPMA (Navon et al. 2003). Thus, the TEM analyses provide additional evidence for the importance of carbonatitic HDF in the formation of the diamonds.

ACKNOWLEDGMENTS

We thank Peter Buseck, Rondi Davies, and Nik Sobolev for constructive reviews, Diavik Mining Corporation, Nik Sobolev, and Alla Logvinova for contributing the diamonds, Elad Izraeli for his help in the EPMA analyses and for good advice, and Alex Rochhol for his help in creating the collaboration. Research was supported by the Israeli Science Foundation (ISF 90/01).

REFERENCES CITED

Beran, A. (2002) Infrared spectroscopy of micas. In A. Mottana, F.P. Sassi, J.B. Thompson, Jr., and S. Guggenheim, Eds., Micas: Crystal Chemistry and Metamorphic Petrology, 46, p. 351–369. Reviews in Mineralogy and Geochemistry, Mineralogical Society of America, Chantilly, Virginia.

Bulanova, G.P. (1995) The formation of diamond. Journal of Geochemical Exploration, 53(1–3), 1–23.

Chrenko, R., McDonald, R., and Darrow, K. (1967) Infra-red spectrum of diamond coat. Nature, 214, 474–476.

Cliff, G. and Lorimer, G. (1975) The quantitative analysis of thin specimens. Journal of Microscopy, 1003, 203–207.

Egerton, R. F. (1996) Electron energy-loss spectroscopy in the electron microscope (2^{nd} ed.), 410 p. Plenum Press, New York.

Giardini, A.A., Hurst, V.J., Melton, C.E., John, C., and Stormer, J. (1974) Biotite as a primary inclusion in diamond: Its nature and significance. American Mineralogist, 59, 783–789.

Guidotti, C.V. (1984) Micas in metamorphic rocks. In S.W. Bailey, Ed., Micas, 13, p. 357–467. Reviews in Mineralogy, Mineralogical Society of America, Chantilly, Virginia.

Gurney, J.J., Harris, J.W., and Rickard, R.S. (1979) Silicate and oxide inclusions in diamonds from the Finsch kimberlite pipe. In F.R. Boyd and H.O.A. Meyer, Eds., Kimberlites, Diatremes and Diamonds: their Geology and Petrology and Geochemistry, vol. 1, p. 1–15. American Geophysical Union, Washington, D.C.

Guthrie, G.D., Veblen, D.R., Navon, O., and Rossman, G.R. (1991) Submicrometer fluid inclusions in turbid-diamond coats. Earth and Planetary Science Letters, 105(1–3), 1–12.

Harris, J. (1992) Diamond Geology. In J. Field, Ed., The Properties of Natural and Synthetic Diamonds, vol. 58A(A–K), p. 384–385. Academic Press, U.K.

Hermann, J. (2003) Experimental evidence for diamond-facies metamorphism in the Dora-Maira massif. Lithos, 70, 163–182.

Hook, S.J. (2000) "Minerals Query", ASTER Spectral Library, 8 Aug 2004, "Name: Phlogopite $KMg_3Si_3AlO_{10}(F,OH)_2$ 2002," 9 Sept 2004, <http://speclib.jpl.nasa.gov/archive/jhu/nicolet/minerals/phyllosilicate/txt/phlogo2s.txt>; "Name: Biotite $K(MgFe^{+2})_3(ALFe^{+3})Si_3O_{10}(OH,F)_2$ 2002," 9 Sept 2004, <http://speclib.jpl.nasa.gov/archive/jhu/nicolet/minerals/phyllosilicate/txt/biotit.txt>.

Hwang, S.-L., Shen, P., Chu, H.-T., Yui, T.-F., Liou, J.G., Sobolev, N.V., and Shatsky, V.S. (2005) Crust-derived potassic fluid in metamorphic microdiamond. Earth and Planetary Science Letters, 231, 295.

Izraeli, E.S., Harris, J.W., and Navon, O. (2001) Brine inclusions in diamonds: a new upper mantle fluid. Earth and Planetary Science Letters, 187, 323–332.

——— (2004) Fluid and mineral inclusions in cloudy diamonds from Koffiefontein, South Africa. Geochimica et Cosmochimica Acta, 68, 2561–2575.

Klein-BenDavid, O., Izraeli, E.S., and Navon, O. (2003a) Volatile-rich brine and melt in Canadian diamonds. 8th International Kimberlite Conference, Extended abstracts, FLA_0109, 22–27 June 2003, Victoria, Canada.

Klein-BenDavid, O., Logvinova, A.M., Izraeli, E., Sobolev, N.V., and Navon, O. (2003b) Sulfide melt inclusions in Yubileinayan (Yakutia) diamonds. 8th International Kimberlite Conference, Extended abstracts, FLA_0111, 22–27 June 2003, Victoria, Canada.

Klein-BenDavid, O., Izraeli, E.S., Hauri, E., and Navon, O. (2004) Mantle fluid evolutionóa tale of one diamond. Lithos, 77, 243–253.

Lang, A.R. and Walmsley, J.C. (1983) Apatite inclusions in natural diamond coat. Physics and Chemistry of Minerals, 9, 6–8.

Logvinova, A.M., Klein-BenDavid, O., Izraeli, E.S., Navon, O., and Sobolev, N.V. (2003) Microinclusions in fibrous diamonds from Yubilenaya kimberlite pipe (Yakutia). In 8th International Kimberlite Conference, extended abstracts, p. FLA_0025, 22–27 June 2003, Victoria, Canada.

Meyer, H.O.A. (1987) Inclusions in diamond. In P.H. Nixon, Ed., Mantle Xenoliths, p. 501–522. Wiley, New York.

Meyer, H.O.A. and McCallum, M.E. (1986) Mineral inclusions in diamonds from the Sloan kimberlites, Colorado. Journal of Geology, 94, 600–612.

Milledge, H., Mendelssohn, M., Woods, P., Seal, M., Pillinger, C., Mattey, D., Carr, L., and Wright, I. (1984) Isotopic variations in diamond in relation to cathodoluminescence. Acta Crystallographica, Section A: Foundations of Crystallography, 40, 255.

Mitchell, R.H. (1995a) Compositional variation of micas in kimberlites, orangeites, lamproites and lamprophyres. In 6th International Kimberlite Conference, Volume 1óKimberlites, related rocks and mantle xenoliths, vol. 38, p. 390–392. Russian Geology and Geophysics, Alberton Press, New York.

——— (1995b) Kimberlites, orangeites, and related rocks, 410 p. Plenum Press, New York.

Mookherjee, M. and Redfern, S.A.T. (2002) A high-temperature Fourier transform infrared study of the interlayer and Si-O-stretching region in phengite-$2M_1$. Clay Minerals, 37, 323–336.

Navon, O. (1991) High internal-pressures in diamond fluid inclusions determined by infrared-absorption. Nature, 353, 746–748.

——— (1999) Formation of diamonds in the Earth's mantle. In J. Gurney, S. Richardson, and D. Bell, Eds., Proceedings of the 7th International Kimberlite Conference, p. 584–604. Red Roof Designs, Cape Town.

Navon, O., Hutcheon, I.D., Rossman, G.R., and Wasserburg, G.J. (1988) Mantle-Derived Fluids in Diamond Microinclusions. Nature, 335, 784–789.

Navon, O., Izraeli, E.S., and Klein-BenDavid, O. (2003) Fluid inclusions in diamondsóthe Carbonatitic connection. 8th International Kimberlite Conference, Extended abstracts, FLA_0107, 22–27 June 2003, Victoria, Canada.

Prinz, M., Manson, D.V., Hlava, P.F., and Keil, K. (1975) Inclusions in diamonds: Garnet lherzolite and eclogite assemblages. Physics and Chemistry of the Earth, 9, 797–815.

Schrauder, M. and Navon, O. (1994) Hydrous and carbonatitic mantle fluids in fibrous diamonds from Jwaneng, Botswana. Geochimica et Cosmochimica Acta, 58, 761–771.

Schrauder, M., Koeberl, C., and Navon, O. (1996) Trace element analyses of fluid-bearing diamonds from Jwaneng, Botswana. Geochimica et Cosmochimica Acta, 60, 4711–4724.

Schreyer, W. (1965) Ein synthetisches Zwischenglied zwischen dioktaedrischen and trioktaedrischen Glimmern. Die Naturwissenschaften, 52, 182–183.

Seifert, F. and Schreyer, W. (1971) Synthesis and stability of micas in the system K_2O-MgO-SiO_2-H_2O and their relations to phlogopite. Contributions to Mineralogy and Petrology, 30, 196–215.

Shatsky, V.S., Sobolev, N.V., and Vavilov, M.A. (1995) Diamond-bearing metamorphic rocks of the Kokchetav massif (Northern Kazakhstan). In R.G. Coleman and X. Wang, Eds., Ultrahigh Pressure Metamorphism, p. 427–455. Cambridge University Press, U.K.

Sobolev, N., Kaminsky, F., Griffin, W., Yefimova, E., Win, T., Ryan, C., and Botkunov, A. (1997) Mineral inclusions in diamonds from the Sputnik kimberlite pipe, Yakutia. Lithos, 39, 135–157.

Stalder, R., Ulmer, P., and Gunther, D. (2002) Fluids in the system forsterite-phlogopite-H_2O at 60 kbar. Schweizerische Mineralogische und Petrographische Mitteilungen, 82, 15–24.

Sunagawa, I. (1984) Morphology of natural and synthetic diamond crystals. In I. Sunagawa, Ed., Materials Science of the Earth's Interior, p. 303–330. Terra Scientific, Tokyo.

Taylor, L.A., Keller, R.A., Snyder, G.A., Wang, W.Y., Carlson, W.D., Hauri, E.H., McCandless, T., Kim, K.R., Sobolev, N.V., and Bezborodov, S.M. (2000) Diamonds and their mineral inclusions, and what they tell us: A detailed "pull-apart" of a diamondiferous eclogite. International Geology Review, 42, 959–983.

Walmsley, J.C. and Lang, A.R. (1992a) On submicrometer inclusions in diamond coatóCrystallography and composition of ankerites and related rhombohedral carbonates. Mineralogical Magazine, 56, 533–543.

——— (1992b) Oriented biotite inclusions in diamond coat. Mineralogical Magazine, 56, 108–111.

Willner, A.P., Herve, F., Thomson, S.N., and Massonne, H.J. (2004) Converging *P-T* paths of Mesozoic HP-LT metamorphic units (Diego de Almagro Island, Southern Chile): evidence for juxtaposition during late shortening of an active continental margin. Mineralogy and Petrology, 81, 43–84.

Wirth, R. (2004) Focused Ion Beam (FIB): A novel technology for advanced application of micro- and nanoanalysis in geosciences and applied mineralogy. European Journal of Mineralogy, 16, 863–876.

Wyllie, P.J. and Ryabchikov, I.D. (2000) Volatile components, magmas, and critical fluids in upwelling mantle. Journal of Petrology, 41, 1195–1206.

MANUSCRIPT RECEIVED NOVEMBER 30, 2004
MANUSCRIPT ACCEPTED AUGUST 22, 2005
MANUSCRIPT HANDLED BY BRIGITTE WOPENKA